
Article:
Pérez-Martín, H., Mackenzie, P., Baidak, A. et al. (2 more authors) (2022) Crystallisation behaviour and morphological studies of PEKK and carbon fibre/PEKK composites. Composites Part A: Applied Science and Manufacturing, 159. 106992. ISSN 1359-835X

https://doi.org/10.1016/j.compositesa.2022.106992

Composites: Part A 159 (2022) 106992

Contents lists available at ScienceDirect

Composites Part A

journal homepage: www.elsevier.com/locate/compositesa

Crystallisation behaviour and morphological studies of PEKK and carbon fibre/PEKK composites

Helena Pérez-Martín [a], Paul Mackenzie [b], Alex Baidak [b], Conchúr M. Ó Brádaigh [a], Dipa Ray [a,*]

[a] School of Engineering, Institute for Materials and Processes, The University of Edinburgh, Edinburgh, United Kingdom
[b] Hexcel Composites Ltd, Duxford, Cambridge, United Kingdom

ARTICLE INFO

Keywords:
A. Polymer-matrix composites (PMCs)
A. Thermoplastic resin
B. Microstructures
B. Thermal properties
CF/PEKK composites
Crystallinity

ABSTRACT

The increased interest in carbon fibre/poly(etherketoneketone) (CF/PEKK) as an option for high-performance applications calls for a thorough understanding of the composite's crystallisation behaviour, due to the essential role that crystallinity plays in performance. In this study, differential scanning calorimetry was used with a variety of thermal cycles to evaluate the effect of thermal history on crystallinity development in unreinforced PEKK and CF/PEKK. Different isothermal holding temperatures during cooling affected the ratio between primary and secondary crystallisation, and non-isothermal cooling cycles influenced the extent of crystallisation. The inclusion of carbon fibres increased the proportion of secondary crystallisation in the matrix and slowed down crystallisation kinetics. A Velisaris-Seferis model was used to model crystallisation kinetics for the isothermal data, and adapted Nakamura models were used for the non-isothermal data. Based on this work, optimum isothermal hold temperatures during cooling for CF/PEKK are estimated to lie in the range of 220–260 °C.

1. Introduction

High-performance, semicrystalline thermoplastics are increasingly being studied as a matrix in structural composites destined for the aerospace industry. Poly(aryletherketones) (PAEKs) in particular, are a family of thermoplastics of interest due to their excellent properties, which also have the added benefit of shorter manufacturing processes that the more conventionally used thermosets lack [1–3]. Due to the higher melt temperatures of PAEK thermoplastics, however, composite manufacturing requires high processing temperatures (350–390 °C). The processing cycle plays a key role in the case of semicrystalline thermoplastic composites, as it controls the extent of crystallinity developed in the material and dictates the mechanical properties [4–6]. Therefore, it is of interest to further investigate the crystallisation behaviour of thermoplastics in order to maintain the performance required for aerospace applications.

Poly(etheretherketone) (PEEK) is the most widely studied polymer of the PAEK family, and has been one of the main candidates as a thermoplastic matrix for high-performance composite applications [1,3,7–10]. Poly(etherketoneketone) (PEKK) has been less studied to date, but is becoming an increasingly attractive option for advanced composites [2,4,11–14]. The reason for this is the difference in ether/ketone ratio between PEEK and PEKK: the ketone-ketone link in PEKK offers a tuneability that PEEK doesn't allow for, where this link can be either para- or meta-, as shown in Fig. 1. The amount of para- to meta-linkages that PEKK contains is commonly referred to as the *T/I ratio*, or *grade*. This is due to its preparation method, combining diphenyl ether (DPE) with terephthalic acid (T), which leads to para- linkages, or with isophthalic acid (I), which creates meta- linkages [2].

The grade has a large effect on the properties of PEKK: a high T/I ratio results in a higher content of *para*-linkages, leading to stiffer molecular chains which in turn allows better chain-packing and a higher melting temperature. This increases viscosity and hinders manufacturing, but results in higher crystallinity and faster crystallisation kinetics due to an increased chain linearity. Conversely, a low T/I ratio will result in more flexible chains and a lower melting temperature, benefitting manufacturability but limiting crystallisation kinetics due to the chain irregularity disrupting crystal packing [15].

The crystallisation mechanism of different PEKK grades has been investigated by several authors [9,11–14,16–19]. Similarly to PEEK, PEKK has been found to crystallise following two distinct crystallisation mechanisms:

* Corresponding author at: 1.140 Sanderson Building, King's Buildings, Edinburgh EH9 3FB, Scotland, UK.
E-mail address: Dipa.Roy@ed.ac.uk (D. Ray).

https://doi.org/10.1016/j.compositesa.2022.106992
Received 17 December 2021; Received in revised form 22 April 2022; Accepted 6 May 2022
Available online 11 May 2022

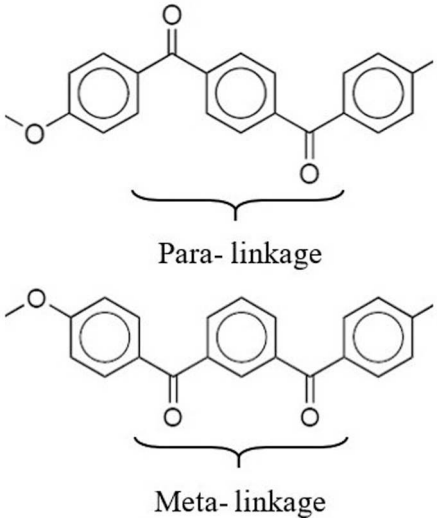

Fig. 1. Molecular structure of PEKK with para- (top) and meta- (bottom) links.

- Primary crystallisation, where amorphous material nucleates and spherulitic growth takes place.
- Secondary crystallisation, where amorphous material between the lamellae of the already established spherulites crystallises.

Fig. 2 depicts these two mechanisms. Spherulitic growth is shown first, indicated by the arrows; and the interlamellar material which undergoes secondary crystallisation is shown magnified.

Literature has highlighted the presence of these two crystallisation modes forming during isothermal holds [2,11–14,16,19,20,22–28]. This is observable in DSC melting curves, where the presence of two (endothermic) melting peaks has been attributed to the dual crystallisation mechanism:

- A higher temperature endotherm (HTE), corresponding to the melting of the primary crystallisation phase (conventional melting). The temperature at which this endotherm takes place is not affected by the isothermal hold temperature.
- A lower temperature endotherm (LTE), associated with the melting of the secondary crystallisation structures. This peak takes place earlier in the heating process, approximately 10–15 °C above the isothermal hold temperature.

Quiroga Cortés et al. [12] observed that the LTE increased in size with higher temperatures and longer holding times of unreinforced PEKK, suggesting an increase in the contribution of secondary crystallisation to the overall crystallisation mechanism. Both peaks contribute towards the total crystallinity of the material. An example of these two peaks is shown in Fig. 3.

However, associating the primary and secondary crystalline phases to the presence of two distinct endothermic peaks poses a limitation in the case of non-isothermal crystallisation studies. In non-isothermal studies of several grades of PEKK by Quiroga Cortés et al. [12] the DSC melting curves showed a single melting endotherm, corresponding to conventional melting (the HTE), as well as a cold crystallisation exotherm, indicating the presence of amorphous material in the samples as a consequence of the faster cooling rates. The absence of an LTE is not addressed in this case. Bessard et al. [24] performed a similar study on PEEK, where they observed a shoulder at the beginning of the single melting endotherm for the slower cooling rates, indicating some contribution from the secondary crystallisation. Similar observations were made by Regis et al. [29] and by Lustiger et al. [30] in their work

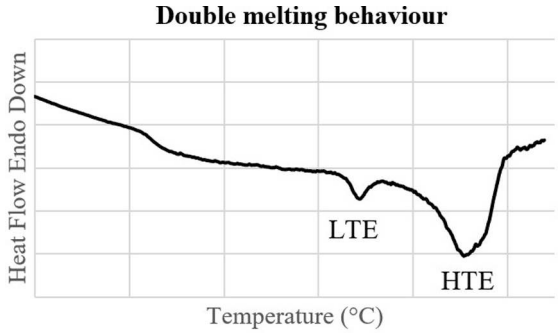

Fig. 3. Representative thermogram of double melting behaviour.

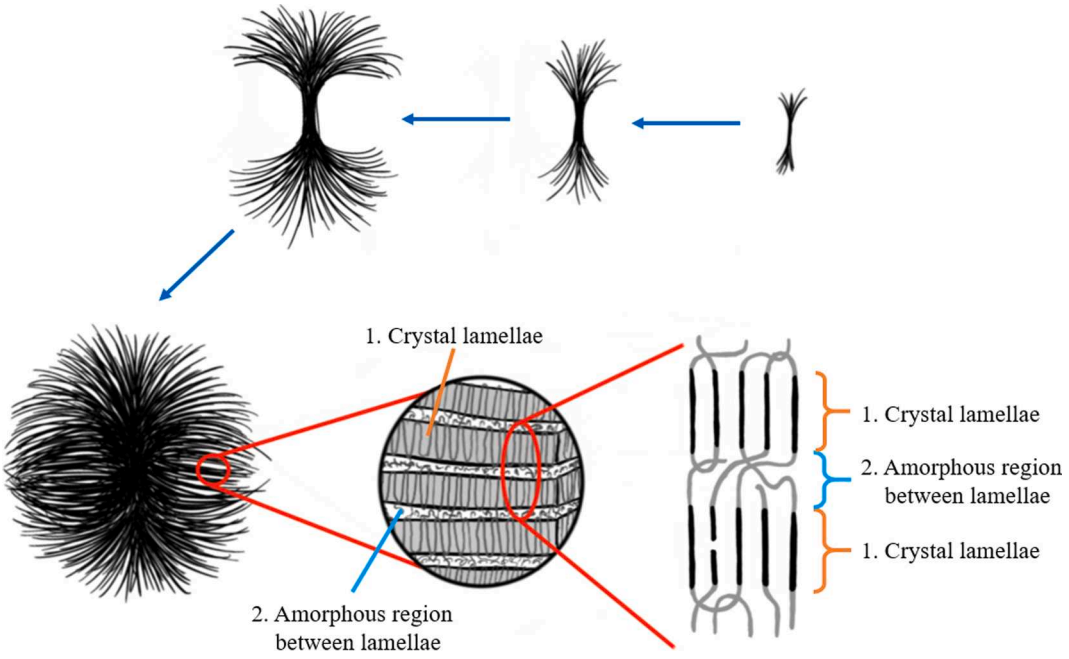

Fig. 2. Schematic depicting spherulitic formation, showing lamellae (crystal) and amorphous regions of a spherulite. Drawn after [2,20,21].

on PEEK and carbon fibre (CF)/PEEK. The presence of secondary crystallisation in slow-cooled PEEK can be explained by the faster kinetics that the PEEK possesses compared to PEKK, due to PEEK's higher chain linearity and lower ketone content. Since the development of secondary crystallisation is determined by time, it is therefore logical that there will be a lower contribution of secondary crystallinity (if at all) at faster cooling rates. The lack on an LTE in non-isothermal PEKK studies may suggest that there is no secondary crystallisation phase present in PEKK after undergoing cooling from the melt, however this has not been explored or discussed in depth to date.

Several studies have integrated both primary and secondary crystallisation mechanisms into crystallisation kinetic models, many of which are based on the Avrami equation [17,22,31,32]:

$$\alpha(t) = 1 - \exp(-kt^n) \tag{1.1}$$

where $\alpha(t)$ is the relative volume fraction crystallinity attained at time t, k is the crystallisation rate constant (which is temperature dependent), and n is the Avrami exponent. Both the crystallisation rate constant and the Avrami exponent are dependent on the nature of the crystallisation, namely the crystalline growth geometry and whether crystallisation is instantaneous or sporadic [2,11,17,33]. k is generally expressed as a function of potential nuclei N and crystal growth rate G. The exact relation is dependent on the nature of crystallisation, and will be defined later in this article. G can be expressed following the Hoffmann-Lauritzen theory [11,34]:

$$G(T) = G_0 \exp\left(-\frac{U^*}{R(T - T_0)}\right)\exp\left(-\frac{K_g}{T\Delta \times T \times f}\right) \tag{1.2}$$

G_0 is a pre-exponential factor independent of temperature. The first exponent contains the contribution of the macromolecular chain diffusion in the melt, whereas the second exponential term corresponds to the contribution of the nucleation process. U^* is the activation energy of the molecular transfer from the melt to the crystal surface, T_∞ is the temperature below which diffusion stops ($T_\infty = T_g - 30$), R is the universal gas constant, K_g is the activation energy of nucleation for a crystal with a critical size, ΔT is the degree of supercooling ($\Delta T = T_m^0 - T$) with T_m^0 as the equilibrium melting temperature, and f is a correction coefficient to account for the temperature dependence of the melting enthalpy ($f = 2T/(T_m^0 + T)$). This model has been successfully implemented to describe crystal growth on PEKK by several authors [11,17,35], and is used later in this article.

It is worth noting, however, that the Avrami equation on its own doesn't allow for the existence of the secondary crystallisation mechanism that takes place in PEKK. This is observable from an Avrami plot, where a plot of $\ln[-\ln(1-\alpha)]$ against $\ln(t)$ will result in a straight line of gradient n and intercept $\ln k$ if the fit is successful. This is not the case for PEKK due to the presence of this secondary mechanism, which is observed later in this article, as well as in literature [11,13]. The most relevant models for dual crystallisation adapt the Avrami equation to take this into account. One of these is the Velisaris-Seferis model [32], in which two separate Avrami crystallisation processes are considered in parallel, representing primary and secondary crystallisation (Eq. (1.3)):

$$\alpha(t) = w_1[1 - \exp(-k_1 t^{n_1})] + w_2[1 - \exp(-k_2 t^{n_2})] \tag{1.3}$$

Subscripts 1 and 2 refer to primary and secondary crystallisation respectively. w_1 and w_2 are weight factors corresponding to each crystallisation mechanism, where $w_1 + w_2 = 1$. This model has been successfully applied to PEEK [32,36], CF/PEEK [32] and PEKK [13].

A different two-stage crystallisation model, originally developed by Hillier and later modified by Hsiao et al. [13] and Choupin et al. [11] has been implemented on PEEK, CF/PEEK and PEKK as well. In this case, the secondary crystallisation is expressed in an integral form. Choupin et al. [17] developed a derivative Hillier model in later work, which has been successfully implemented on unreinforced PEKK. A more thorough explanation of the above can be found in the cited articles, as well as in [2].

The Velisaris-Seferis model is adequate for isothermal crystallisation modelling, however in non-isothermal instances, the variation of the crystallisation rate constant k with respect to temperature must be accounted for. This was carried out by Nakamura in their adaptation of the Avrami equation as follows [37]:

$$\alpha(t) = 1 - exp\left[-\left(\int_0^t K\, dt\right)^n\right] \tag{1.4}$$

where K is temperature dependent and connected with the isothermal crystallisation rate constant k through the relation:

$$K = k^{1/n} \tag{1.5}$$

An equation for K can therefore be determined by first finding a temperature-dependent equation for k based on isothermal crystallisation experiments and the Hoffmann-Lauritzen model, and then substituting into Eq. (1.5).

As per the Avrami equation, the Nakamura model only takes into account a single crystallisation mechanism. In a similar manner to the Velisaris-Seferis model, the secondary mechanism can be accounted for by having two separate Nakamura models acting in parallel:

$$\alpha(t) = w_1\left(1 - exp\left[-\left(\int_0^t k_1^{1/n_1} dt\right)^{n_1}\right]\right) + w_2\left(1 - exp\left[-\left(\int_0^t k_2^{1/n_2} dt\right)^{n_2}\right]\right) \tag{1.6}$$

with substitutions for K_1 and K_2 as shown in Eq. (1.5). Bessard et al. [24] used a differential form of Eq. (1.6) to model non-isothermal crystallisation kinetics of unreinforced PEEK. Their investigation resulted in a successful fit where a gradual decrease in the secondary crystallisation contribution to the total crystallinity was observed with a faster cooling rate.

Despite this understanding of the crystallisation mechanisms, kinetics and modelling of different grades of PEKK developed by several authors, an investigation and comparison of crystallisation between unreinforced PEKK and CF/PEKK has not been performed in depth. Some published literature discussing the impact of carbon fibres on crystallinity development is available for PEEK, where fibre inclusions were found to decrease overall crystallinity [5]. Research on kinetics is somewhat inconclusive, where some work proposes that the inclusion of fibres has no major effect on PEKK crystallisation kinetics [13], but other research suggests that this varies with isothermal temperature hold, leading to faster kinetics in composite samples at higher temperatures (reported in theses work on PEEK [38] and PEKK [39]). These are discussed in more detail in [2].

Further to this, the discussion of dual crystallisation kinetics during non-isothermal crystallisation is sparse, now that a secondary crystallisation peak is not obvious in heat scans performed in literature. Consequently, non-isothermal crystallisation models are sparsely implemented on PEKK compared to isothermal ones.

This article offers a detailed study of PEKK with a T/I ratio of 70/30 in both unreinforced and composite forms, undergoing a variety of isothermal and non-isothermal cycles in order to study the effect of carbon fibre inclusions on the crystallisation mechanism and kinetics. The Velisaris-Seferis and dual Nakamura models discussed above are then implemented to interpret the results. This work first covers the crystallinity, morphology, kinetics and modelling of the isothermal cycles that unreinforced and composite PEKK are exposed to, followed by the non-isothermal studies and models. A brief discussion focussing on the relevance of this work in high-performance thermoplastic composite applications is also included.

2. Material and methods

2.1. Materials

In this study, KEPSTAN PEKK 7002PT by Arkema is used in powder form, provided by Hexcel Composites Ltd. This grade of PEKK has a T/I ratio of 70/30, with glass transition temperature and melting temperature measured at 161 °C and 338 °C respectively. This grade in particular is intended for the manufacturing of unidirectional prepreg tape with carbon fibres [40].

The composite material used is unsized AS7 CF/PEKK unidirectional prepreg tape, provided by Hexcel Composites Ltd. The PEKK matrix in the tape is the same grade as the powder. The fibre volume fraction of the prepreg material was measured to be 60.8% by acid digestion (68.3% fibre weight content).

2.2. Differential scanning calorimetry (DSC)

Isothermal and non-isothermal crystallisation analyses were carried out using a PerkinElmer DSC 8000, with aluminium pans non-hermetically sealed with aluminium lids. Indium was used to calibrate the temperature and heat of fusion prior to any experiments. Sample weights of 5–7 mg of neat PEKK powder were used, whereas sample weights of 10–12 mg of CF/PEKK prepreg tape were used. All experiments were run twice in order to ensure repeatability, and under a nitrogen environment to avoid any sample degradation.

In order to erase any thermal history, samples were initially heated to 370 °C, and held in the melt for 5 min. For isothermal analysis, samples were cooled at a rate of 150 °C/min down to the temperature of interest (220, 240, 260, 280, or 300 °C), held for 60 min, and then further cooled at a rate of 150 °C/min to room temperature. For non-isothermal crystallisation analysis, samples were cooled at the rate of interest (5, 10, 20, 40, 60, 100 or 150 °C/min) from the melt to room temperature. All samples then underwent a second heat ramp at 20 °C/min to measure the effect of the crystallisation cycle on the glass transition, melting temperature and crystallinity. The temperature–time plots of these thermal cycles are shown in Fig. 4.

Performing the second heat ramp at the end of the cycle removes all thermal history. In order to later observe the impact of the thermal history at microscopic scale under scanning electron microscopy (SEM), CF/PEKK samples underwent the same cycle once again with the exception of the final heating ramp.The crystallinity of a sample can be estimated with:

$$\chi = \frac{\Delta H_m - \Delta H_{cc}}{\alpha \times \Delta H_{100\%}} \tag{2.1}$$

where ΔH_m is the melting enthalpy, ΔH_{cc} is the cold crystallisation enthalpy, α is the weight fraction of matrix content (100% in the case of the unreinforced PEKK powder, 31.7% in the case of CF/PEKK prepreg tape) and $\Delta H_{100\%}$ is the theoretical melting enthalpy of 100% crystalline PEKK. This has been calculated to be 130 J/g by Chang and Hsiao [16].

2.3. Scanning electron microscopy

SEM was performed on cryofractured CF/PEKK prepreg tape samples after undergoing the DSC cycles described above, in order to qualitatively examine the effect that crystallinity had on fibre–matrix interfacial adhesion and matrix morphology. Cryofracture involved submerging the samples in liquid nitrogen, followed by fracturing to expose their cross-section. Samples were prepared with a 15 nm sputter coating of gold to enhance surface conductivity, and then imaged with a JEOL JSM-IT100 instrument at 20 kV.

3. Results and discussion

3.1. Isothermal crystallisation

3.1.1. Crystallisation at different isothermal temperatures

Fig. 5 shows the heat flow variation of one set of runs of unreinforced PEKK powder and CF/PEKK prepreg tape, during a heat ramp of 20 °C/min from room temperature to 370 °C, after undergoing different isothermal temperatures from the melt held for 60 min. Table 1 shows average data from this portion of the cycle for both performed runs.

Two melting endotherms are observed in the heat scans in Fig. 5, corresponding to the LTE and HTE as discussed in Section 1. The LTE is approximately 15 °C above the isothermal temperature throughout for both unreinforced and composite PEKK. In the case of the 280 °C and 300 °C isothermal holds where the two endotherms overlap, the area corresponding to each endotherm was calculated by drawing a line perpendicular to the baseline, crossing the curve at its inflection point between the two peaks. This is illustrated on the 300 °C isothermal curve in Fig. 5a.

As the isothermal hold temperature increases, the LTE:HTE ratio can be seen to increase, the variation of which can be observed in Table 1 and Fig. 6. The reasoning for this may be as follows. In order for secondary crystallisation to take place, primary crystallisation (formation of spherulites) must be established first. As primary crystallisation takes

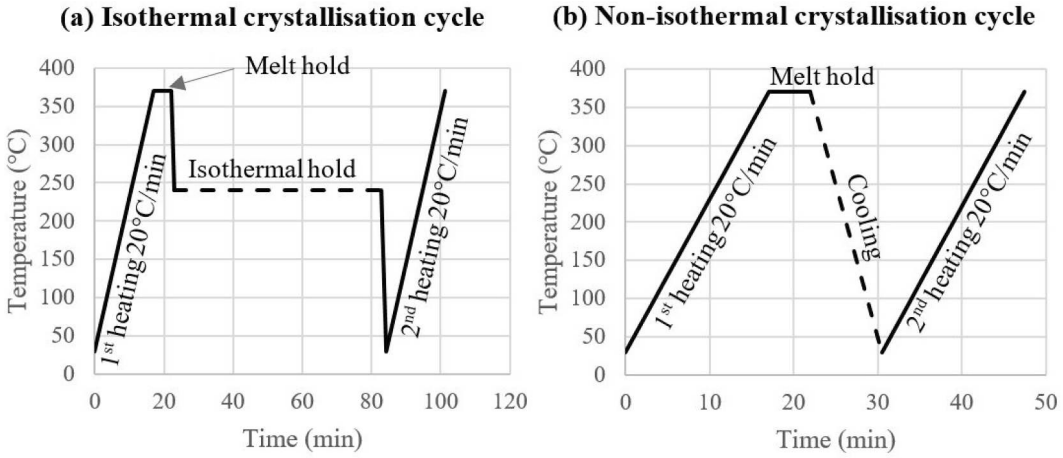

Fig. 4. DSC heat cycle of all samples undergoing (a) isothermal crystallisation analysis and (b) non-isothermal or dynamic crystallisation analysis. The dotted sections of the plot indicate (a) the isothermal hold of the cycle, which can be at 220, 240, 260, 280 or 300 °C; and (b) the cooling section of the cycle, which can be 5, 10, 20, 40, 60, 100 or 150 °C/min cooling rate.

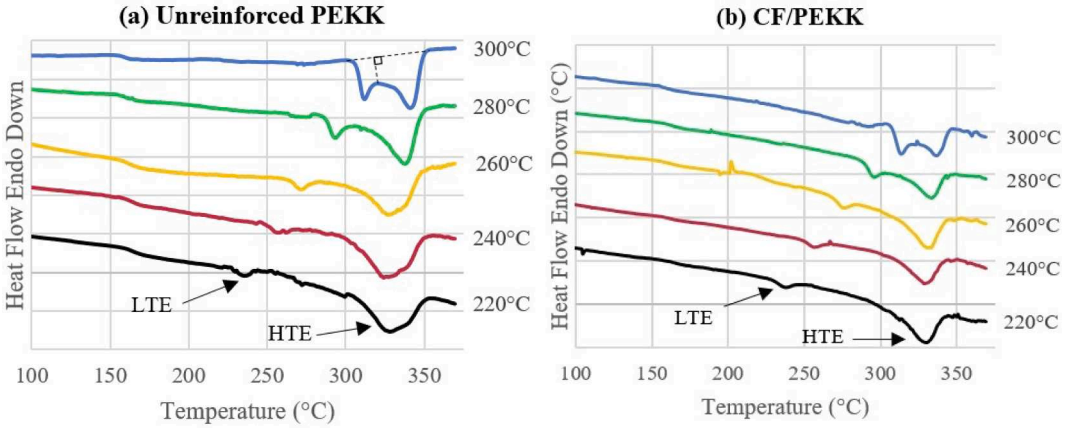

Fig. 5. DSC thermograms (second heating cycles in Fig. 4a) of (a) unreinforced PEKK powder and (b) CF/PEKK prepreg tape after undergoing isothermal crystallisation at different temperatures with a hold time of 60 min. Dotted lines in the 300 °C curve in (a) demonstrate how the area corresponding to each endotherm (LTE and HTE) was calculated in instances where the two peaks overlap.

Table 1
Average values for transition temperatures, melting enthalpies and total crystallinity of unreinforced PEKK powder and CF/PEKK prepreg tape after undergoing different isothermal holds.

Isothermal temp. (°C)	Unreinforced PEKK						
	T_g (°C)	T_{LTE} (°C)	ΔH_{LTE} (J/g)	T_{HTE} (°C)	ΔH_{HTE} (J/g)	LTE:HTE	χ (%)
220	165.5 ± 1.1	239.6 ± 4.4	1.8 ± 0.2	328.6 ± 0.5	29.7 ± 0.1	5:95 ± 1	24.2 ± 0.2
240	163.5 ± 0.3	258.4 ± 2.0	2.3 ± 0.3	324.0 ± 0.2	29.1 ± 0.4	7:93 ± 1	24.1 ± 0.2
260	162.0 ± 0.8	274.9 ± 3.3	2.5 ± 0.2	331.9 ± 5.0	26.9 ± 0.2	8:92 ± 1	22.6 ± 0.1
280	159.7 ± 0.8	298.1 ± 4.9	7.3 ± 0.3	337.5 ± 0.1	28.4 ± 0.4	20:80 ± 1	27.5 ± 0.5
300	158.5 ± 0.1	315.5 ± 3.8	10.4 ± 0.5	341.7 ± 0.5	20.4 ± 1.8	34:66 ± 3	23.7 ± 1.1
				CF/PEKK			
220	164.3 ± 0.9	239.8 ± 2.1	1.0 ± 0.1	329.4 ± 0.3	9.1 ± 0.1	10:90 ± 0	24.3 ± 0.6
240	158.5 ± 1.8	258.9 ± 2.5	1.1 ± 0.2	329.2 ± 0.3	8.5 ± 0.1	10:90 ± 1	23.0 ± 0.5
260	160.4 ± 1.4	277.0 ± 1.2	1.1 ± 0.2	334.1 ± 2.7	8.2 ± 0.5	12:88 ± 1	22.5 ± 1.5
280	159.6 ± 2.8	300.4 ± 5.0	3.1 ± 0.4	335.5 ± 2.2	7.9 ± 0.1	28:72 ± 2	26.6 ± 1.2
300	161.4 ± 2.0	316.3 ± 2.8	4.7 ± 0.5	338.8 ± 2.1	5.2 ± 0.1	47:53 ± 3	23.7 ± 1.0

T_g: Glass transition temperature.
T_{LTE}: Low temperature endotherm.
ΔH_{LTE}: Low temperature endotherm enthalpy.
T_{HTE}: High temperature endotherm.
ΔH_{HTE}: High temperature endotherm enthalpy.
LTE:HTE: Low temperature endotherm to high temperature endotherm ratio.
χ: Total crystallinity.

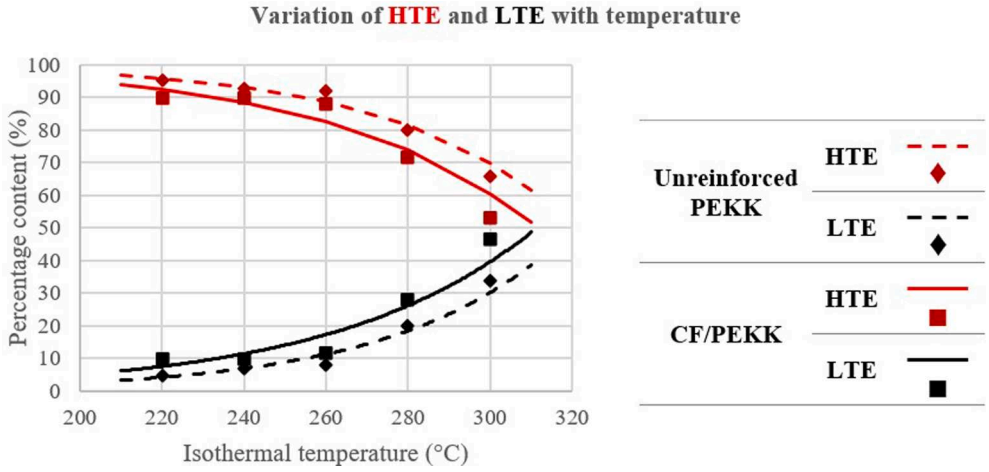

Fig. 6. Variation of LTE and HTE with isothermal temperature for unreinforced PEKK powder and CF/PEKK prepreg tape. Solid and dotted lines are exponential lines of best fit.

place and spherulites develop, the spherulites' lamellae expand and branch out, becoming larger and therefore creating more interlamellar space for secondary crystallisation to happen. The extent to which spherulites grow is determined by general polymeric nucleation theory, where at lower temperatures the formation of new spherulite nuclei takes precedence over spherulitic growth. This results in a high number of small spherulites. On the other hand, at higher temperatures, spherulitic growth predominates over the formation of new nuclei, resulting in a smaller number of spherulites but larger in size. It is therefore possible that, at higher isothermal temperatures, there is more interlamellar space created by the larger spherulites, allowing for a larger volume of interlamellar growth (secondary crystallisation) to take place than at low isothermal temperatures. This therefore results in a larger presence of secondary crystallites, and a larger LTE:HTE endotherm ratio. A schematic portraying this is shown in Fig. 7.

From the above results in Table 1 and Fig. 6, it can also be observed that CF/PEKK has a slightly larger LTE:HTE ratio than the unreinforced PEKK (a higher presence of secondary crystallisation) throughout all isothermal hold temperatures. A possible reason for this could be the presence of densely-packed fibres supressing spherulitic development, causing a slower growth of the primary crystallisation phase in CF/PEKK compared to the neat samples at a given time *t*, as shown in Fig. 8.

Spherulitic growth is governed by primary crystallisation, which in turn affects the extent to which secondary crystallisation can take place. However, secondary crystallisation takes place at a smaller scale and does not require major molecular rearrangement in the manner that primary crystallisation does (since it occurs in already established interlamellar regions), and it is therefore possible that it *locally* progresses at the same speed as in the unreinforced case. This would result in a larger percentage of the crystallinity contribution in CF/PEKK being from the secondary phase, resulting in a larger LTE:HTE ratio as seen in Fig. 6.

Another potential explanation for the larger proportion of the LTE could be a different nucleation density and crystal growth at the fibre surface. Fibres may be a source of heterogeneous nucleation and transcrystallinity, which may possess a higher fraction of secondary crystallisation than spherulites developed in the bulk of the matrix via homogeneous nucleation.

Fig. 9a, b and c show SEM images of cryofractured CF/PEKK samples after undergoing the previously described DSC isothermal cycles at 220, 260 and 300 °C respectively. Spherulite structures can be observed in Fig. 9c, these becoming smaller and slightly less defined in Fig. 9b and even less so in Fig. 9a. As described previously, higher isothermal hold temperatures induce a lower nucleation density and larger spherulitic growth, which is the case in the 300 °C isotherm. Consequently, the largest and most defined spherulites can be observed in Fig. 9c. On the other hand, at lower isothermal temperatures, nucleation density is higher and therefore smaller spherulites are formed due to an early impingement between growth fronts. This may be the reason why spherulitic structures in Fig. 9a are the least defined. However, this could also be due to the proximity of the fibres limiting the crystallisation to purely perpendicular to the fibre surface.

Another potential explanation for the matrix morphology seen in these figures is the presence of transcrystallinity. It is possible that with lower isothermal hold temperatures, the growth of a transcrystalline interface is incentivised as a consequence of primary nucleation dominating at lower temperatures and the fibre surfaces inducing such nucleation. In Fig. 9b (260 °C isotherm), some epitaxial growth can be observed perpendicular to the fibre surfaces, which then seem to change orientation and form more spherulite-like structures in the bulk. In Fig. 9a, this perpendicular growth seems to be the most obvious.

3.1.2. *Crystallisation kinetics at different isothermal holds*

Fig. 10 shows heat flow – time thermograms of unreinforced PEKK and CF/PEKK samples during the DSC isothermal holds. Crystallisation occurs in the first minutes of the isothermal hold, and therefore only the first 20 min of the 60-minute hold are shown (minutes 20–60 do not show any variation in heat flow).

In the case of unreinforced PEKK, crystallisation kinetics curves for 220 °C and 240 °C are not present and the peak for 260 °C is only partially present. This is because unreinforced PEKK is partially crystallised when reaching these isothermal temperatures. When cooling from the melt at 150 °C/min, crystallisation takes place in the temperature range 260–210 °C (shown later in Fig. 17a in Section 3.2.2, where crystallisation kinetics under non-isothermal conditions is discussed). By the time that the isothermal temperature (240 or 220 °C) is reached when cooling from the melt, crystallisation has already occurred. Therefore, when the isotherm hold begins, there is no crystallisation

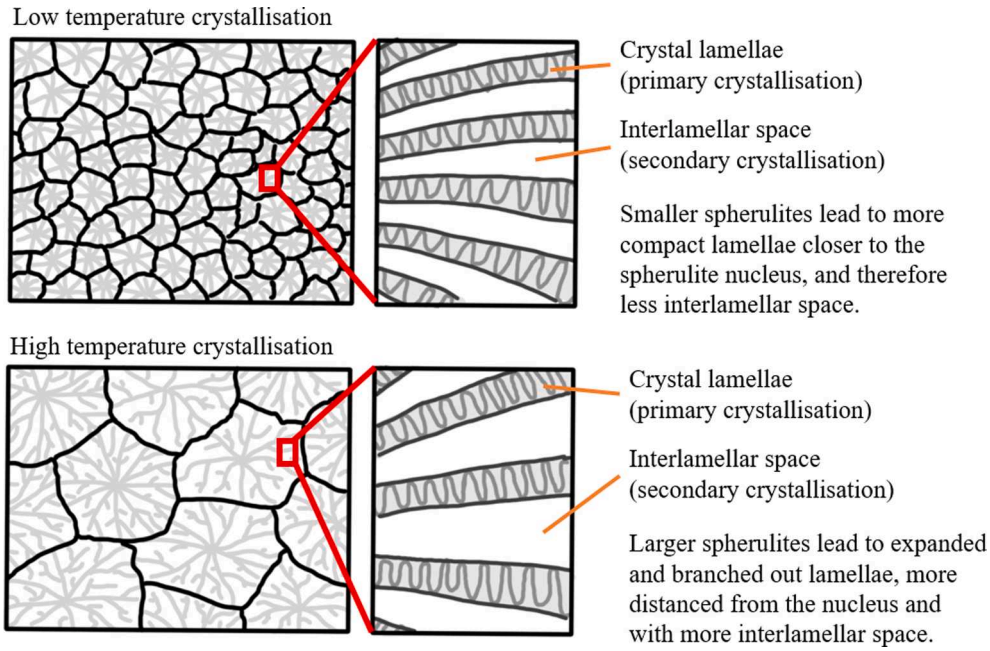

Fig. 7. Schematic showing spherulite size at low and high temperature isotherms, and the consequent interlamellar spacing in which secondary crystallisation takes place.

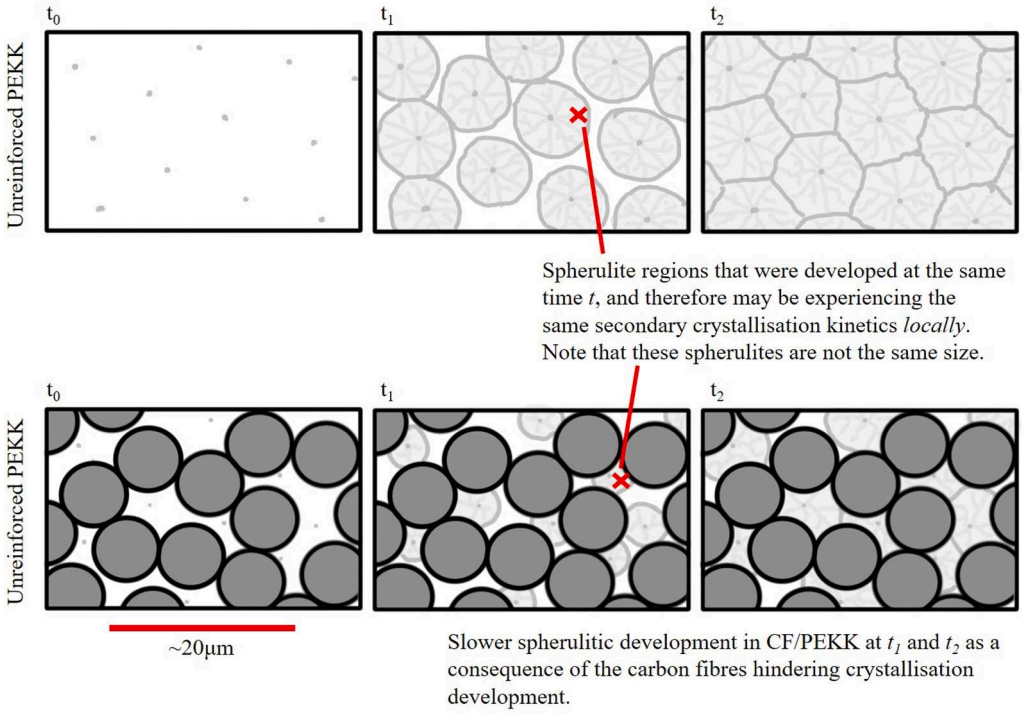

Fig. 8. Schematic representation of spherulitic development in unreinforced PEKK and CF/PEKK, depicting the difference in growth kinetics at different times as a consequence of CFs inhibiting spherulitic growth. Schematics of CF/PEKK are based on an SEM micrograph of the cross-section of a CF/PEKK prepreg sample. The regions marked with an X indicate areas in the two different samples that crystallised at the same time t.

taking place. In order to assess the crystallisation kinetics at the lower isotherms, a faster cooling rate would have to be applied. Kinetics and modelling of unreinforced PEKK will therefore only be discussed for the isothermal holds at 260, 280 and 300 °C henceforth.

Other authors have assessed the crystallisation kinetics of unreinforced PEKK in literature. Choupin et al. [17] used KEPSTAN PEKK 7002 in their studies, a similar grade of PEKK with the same T/I ratio as the one used in this article (KEPSTAN PEKK 7002PT). While they found peak kinetics to take place at approximately 245 °C (which would be in line with this article's results), kinetics were considerably slower. They observed a clear crystallisation peak at ~ 0.8 min during an isothermal hold of 250 °C after cooling at 40 °C/min, a cooling rate which they determined was fast enough to not result in any crystallisation before reaching the isothermal temperature. This is not the case in this study, where both unreinforced and composite PEKK do crystallise at rates above 40 °C/min, as will be shown in Section 3.2.

In a different article, Chelaghma et al. [35] used KEPSTAN PEKK 7003, which also possesses a T/I ratio of 70/30 but has a lower viscosity than the KEPSTAN PEKK 7002 series [15]. This material still displayed slower crystallisation kinetics (~1.8 min peak time at 270 °C) than the grade being studied in this article (~0.5 min peak time at 280 °C). This may be a consequence of different syntheses or modifications of the different grades, as they are intended for different applications [40].

A comparison of the rest of the unreinforced PEKK isothermal holds with their composite counterparts clearly revealed that CF/PEKK has slower crystallisation kinetics, peaking between 240 and 260 °C. This is likely due to the high carbon fibre content hindering the growth and development of spherulites as previously discussed, resulting in slower kinetics. Hsiao et al. [13] found peak kinetics to take place at 255 °C and reported minimal impact of fibres on the crystallisation rate of PEKK under isothermal conditions, however there could be differences in the matrix composition, which in Hsiao et al.'s case was provided by DuPont. It is also possible that the different carbon fibres used (AS4 carbon fibres in Hsiao et al.'s work) cause the difference in results.

3.1.3. Modelling of isothermal crystallisation kinetics

In order to implement the Velisaris-Seferis model discussed in Section 1, a plot of the relative crystallinity of each sample against time is needed. This can be obtained by dividing the area under the curves in Fig. 10 at time t by the area under the entire curve. This is defined by Eq. (3.1):

$$\alpha(t) = \frac{\int_0^t Q(t)dt}{\int_0^{t_\infty} Q(t)dt} \tag{3.1}$$

where $Q(t)$ is the heat flow measured at time t, and t_∞ is the time when the polymer is fully crystallised. The resulting relative crystallinity-time curves are shown in Fig. 11. In the cases where some data points at the beginning of the isothermal crystallisation exotherm are missing in Fig. 10 as a consequence of partial crystallisation during the cooling step, the curves shown in Fig. 11 do not start at a relative volume crystallinity of 0.

Avrami plots can be obtained by plotting $\ln[-\ln(1-\alpha)]$ against $\ln(t)$, shown in Fig. 12. As discussed in Section 1, these do not provide a straight line of best fit, implying that there is more than a single crystallisation mechanism taking place. An estimated Avrami exponent for the primary crystallisation stage can be obtained by calculating the slope of the first part of the curves [11,13,32].

In the case of unreinforced PEKK, the linear sections of the plots average to 2.9, making 3 the closest integer. This is in line with the instantaneous nature of crystallisation, as observed by other authors in hot stage microscopy [11,35], as well as its three-dimensional, spherulitic form. For CF/PEKK however, these slopes average to 2.5. A potential cause for this could be restricted growth as a consequence of fibre proximity, which may limit the three-dimensional spherulitic growth in the matrix bulk, inducing early impingement and reducing the value of n_1. High nucleation density on the fibre surface may be another reason for the lower n_1 value: this may cause a transcrystalline region, which resembles a unidirectional growth from the nucleation site as opposed to the three-dimensional growth of spherulites in the bulk.

Values for n_2 were not determined from the Avrami plots in Fig. 12,

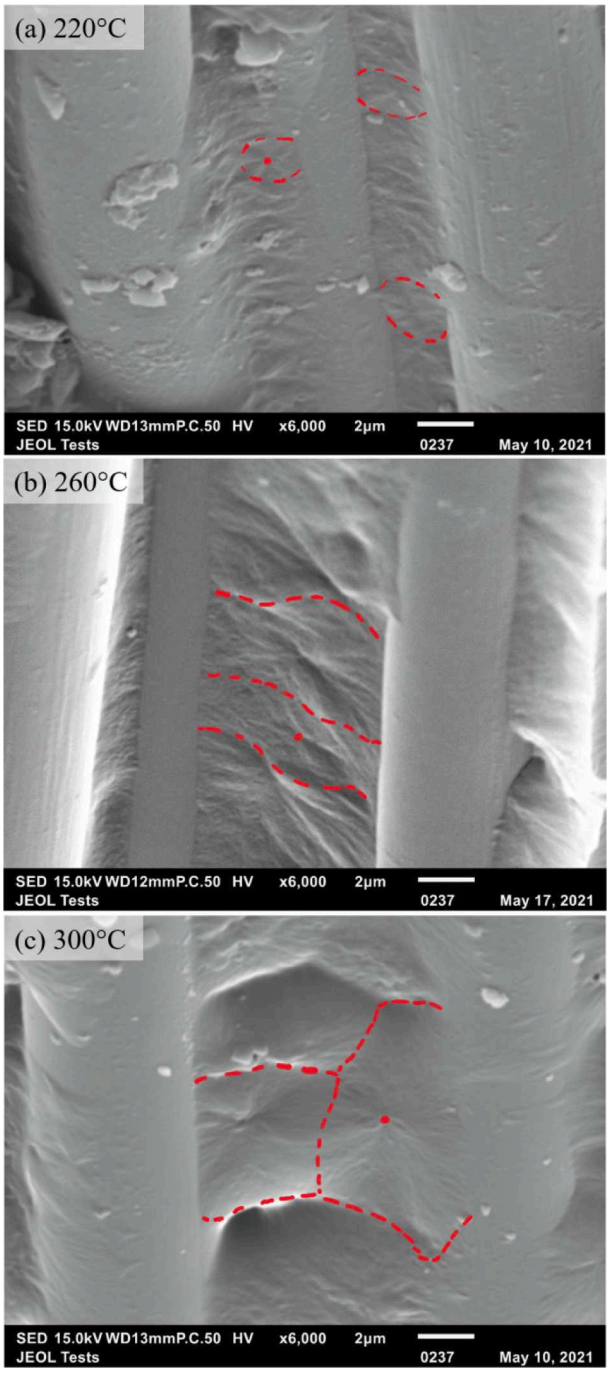

Fig. 9. SEM of cryofractured CF/PEKK samples after undergoing an isothermal hold of (a) 220 °C, (b) 260 °C and (c) 300 °C from the melt. Red annotations highlight spherulitic structures, with a red dot providing an example of a nucleus location. (For interpretation of the references to colour in this figure legend, the reader is referred to the web version of this article.)

now that the gradients obtained at the upper tail of the curves varied between 0.6 and 0.8, and these proved to provide very poor fits. Further to this, other authors have used both integer and non-integer values ranging between 1 and 3 to model secondary crystallisation kinetics of PEEK and PEKK with Avrami-based models [17,22,32,35]. This value would be picked based on which one provided the best fit with the experimental data, and some authors allowed the value for n_2 to vary with the isothermal hold temperature [28]. This further highlights the more complicated nature of secondary crystallisation, which suggests that the growth of secondary crystallisation structures may consist of different dimensions, the proportions of which may vary with isothermal holding temperature.

For modelling purposes, the Avrami exponents (n_1 and n_2) were kept constant across different temperatures in this work. The Velisaris-Seferis model was scripted in MATLAB, setting n_1 to 3 and 2.5 for unreinforced and composite PEKK respectively. A value for n_2 was determined by the script that provided the best fit for all curves, which for both unreinforced and composite PEKK was $n_2 = 2$. w_1 and w_2 were set according to the LTE:HTE ratios calculated in Table 1 for each individual isotherm. k_1 and k_2 were optimised by the script using a non-linear least squares method. All parameters are summarised in Table 2.

The obtained models are shown in Fig. 13. The Velisaris Seferis model (solid lines) achieves a good fit with the provided Avrami exponents (n_1 and n_2) and weight factors (w_1 and w_2), and with the optimised crystallisation rate constants (k_1 and k_2). The contributions of the primary and secondary crystallisations to the overall model are depicted by the different dotted lines in the plots.

Plots showing the variation of $\ln(k_1)$ and $\ln(k_2)$ against the isothermal temperatures are shown in Fig. 14. Hoffmann-Lauritzen models were fitted to these values, which will be used when modelling crystallisation kinetics at different cooling rates in Section 3.2.3. The equations for these curves are summarised below.

For spherulitic growth during primary crystallisation, k_1 is expressed as per Eq. (3.2), which results in the Hoffmann-Lauritzen model in Eq. (3.3) used in Fig. 14a.

$$k_1 = \frac{4}{3}\pi N_{01} G_1^3 \tag{3.2}$$

$$k_1 = k_{01}\left[\exp\left(-\frac{3U^*}{R(T-T_\infty)}\right) \times \exp\left(-\frac{3K_{g1}}{T\Delta Tf}\right)\right] \tag{3.3}$$

where $k_{01} = \frac{4}{3}\pi N_{01} G_{01}^3$. G_1 is the crystal growth rate described in Eq. (1.2), N_{01} is the initial number of potential nuclei and G_{01} is a pre-exponential factor independent of temperature.

For crystal growth during secondary crystallisation, k_2 is expressed as per Eq. (3.4) and Eq. (3.5), used in Fig. 14b.

$$k_2 = \pi N_{02} G_2^2 \tag{3.4}$$

$$k_2 = k_{02}\left[\exp\left(-\frac{2U^*}{R(T-T_\infty)}\right) \times \exp\left(-\frac{2K_{g2}}{T\Delta Tf}\right)\right] \tag{3.5}$$

where $k_{02} = \pi N_{02} G_{02}^2$. Parameter definitions are as per Eqs. (3.2) and (3.3). Table 3 provides the parameters used for the models, as well as results for k_{01}, k_{02}, K_{g1} and K_{g2}. Note that, while all temperature values are given in °C, modelling was performed with temperature in units of Kelvin.

Fig. 14a and Fig. 14b show slower crystallisation kinetics for the secondary crystallisation mechanism k_2, due to this step requiring an established primary crystallisation and a longer time to develop. This is in line with what was previously discussed in Section 1.

Hoffmann-Lauritzen model fitting show that the fastest crystallisation kinetics for both unreinforced PEKK and PEKK composites occur at circa 255 °C and 260 °C for k_1 and k_2 respectively. This is in line with what has been reported in literature to date, where the fastest kinetics were identified to take place at approximately 255 °C [13].

3.2. Non-isothermal crystallisation

3.2.1. Crystallisation at different cooling rates

Fig. 15 shows the heat flow variation of one set of runs of PEKK powder and CF/PEKK respectively, when heated from room temperature to 370 °C at a rate of 20 °C/min, after undergoing different cooling rates. Table 4 shows average data from this portion of the cycle for both performed runs.

The crystallinity of unreinforced PEKK powder decreases with an

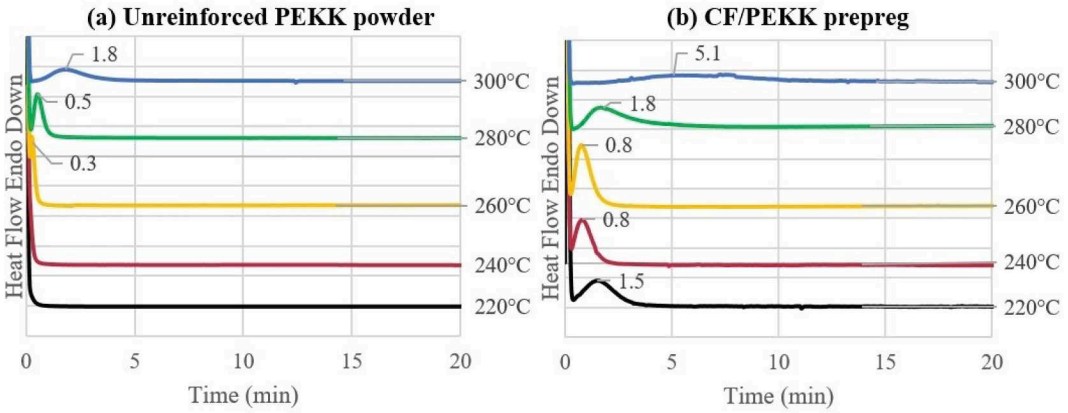

Fig. 10. DSC thermograms of (a) unreinforced PEKK powder and (b) CF/PEKK prepreg tape while undergoing isothermal holds at different temperatures showing peak crystallisation kinetics times in minutes.

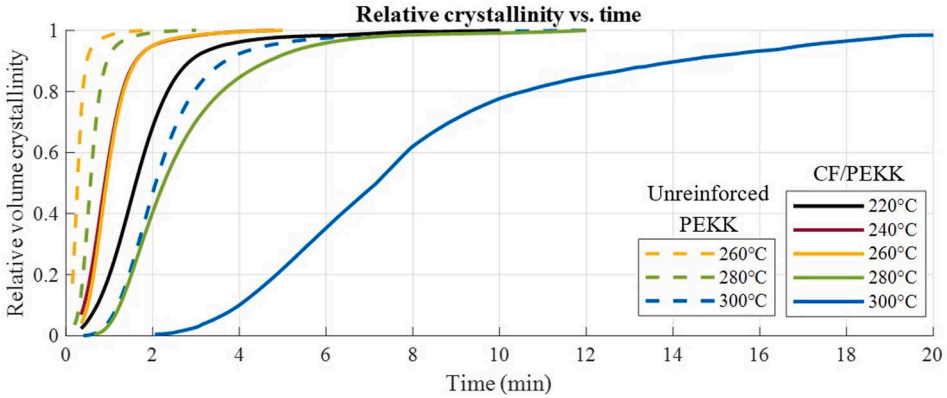

Fig. 11. Relative crystallinity against time of unreinforced PEKK (dotted lines) and CF/PEKK (solid lines) at different isothermal holds.

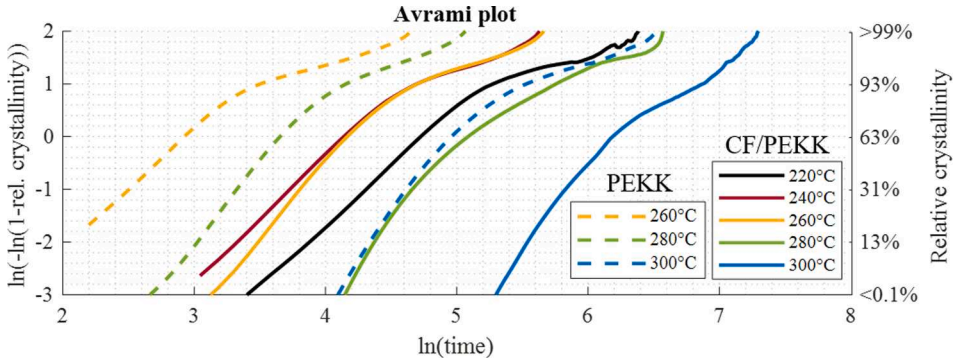

Fig. 12. Avrami plots of the relative crystallinity of unreinforced PEKK and CF/PEKK.

increase in cooling rate, due to faster temperature drops inhibiting chain movement and therefore limiting diffusion onto the growing crystal front [5]. There is therefore a small cold crystallisation peak developed at the faster cooling rates (100 °C/min, 150 °C/min). This agrees with results from Quiroga Cortés et al. [12], where this peak takes place at the fastest cooling rates across different PEKK grades.

The crystallinity of CF/PEKK, on the other hand, is affected more significantly by the cooling rate, as is observable from Table 4. An increasingly larger cold crystallisation peak develops with higher cooling rates in Fig. 15b, and therefore a drop in crystallinity from 25.7% at 5 °C/min to 1.5% at 150 °C/min takes place. This drastic difference is likely due to carbon fibres suppressing spherulitic development as discussed in Section 2, which becomes increasingly significant at faster cooling rates. It is possible that, while carbon fibre surfaces can act as nucleation sites, densely packed fibres are likely to supress chain mobility and spherulitic growth, and will have a larger impact in the overall crystallisation. Similar observations were made by Gao and Kim [5] when evaluating the impact of CF inclusions on the crystallisation capability of PEEK. They observed lower crystallinities in CF/PEEK with a fibre volume fraction of 61% in comparison to PEEK powder when undergoing different cooling rates.

As discussed in Section 1, the characteristic double melting endotherm observed in Fig. 5 is not present during non-isothermal crystallisation. This absence could be a consequence of secondary crystallisation being a slower mechanism that requires an established primary crystallisation and time to develop, both of which are reduced

Table 2
Summary of Velisaris-Seferis model parameters for the isothermal crystallisation modelling of unreinforced PEKK and CF/PEKK. w_1 and w_2 are extracted from the LTE: HTE ratios in Table 1.

Isothermal temperature (°C)	Unreinforced PEKK ($n_1 = 3$, $n_2 = 2$)				CF/PEKK ($n_1 = 2.5$, $n_2 = 2$)			
	w_1	w_2	k_1	k_2	w_1	w_2	k_1	k_2
220	–	–	–	–	0.90	0.10	0.2363	0.0556
240	–	–	–	–	0.90	0.10	1.0109	0.1914
260	0.92	0.08	38.8591	1.3068	0.88	0.12	0.9123	0.2539
280	0.80	0.20	4.3684	1.0171	0.74	0.26	0.1107	0.0472
300	0.69	0.31	0.0961	0.0838	0.55	0.45	0.0069	0.0084

w_1: primary crystallisation weight factor.
w_2: secondary crystallisation weight factor.
k_1: primary crystallisation rate constant.
k_2: secondary crystallisation rate constant.

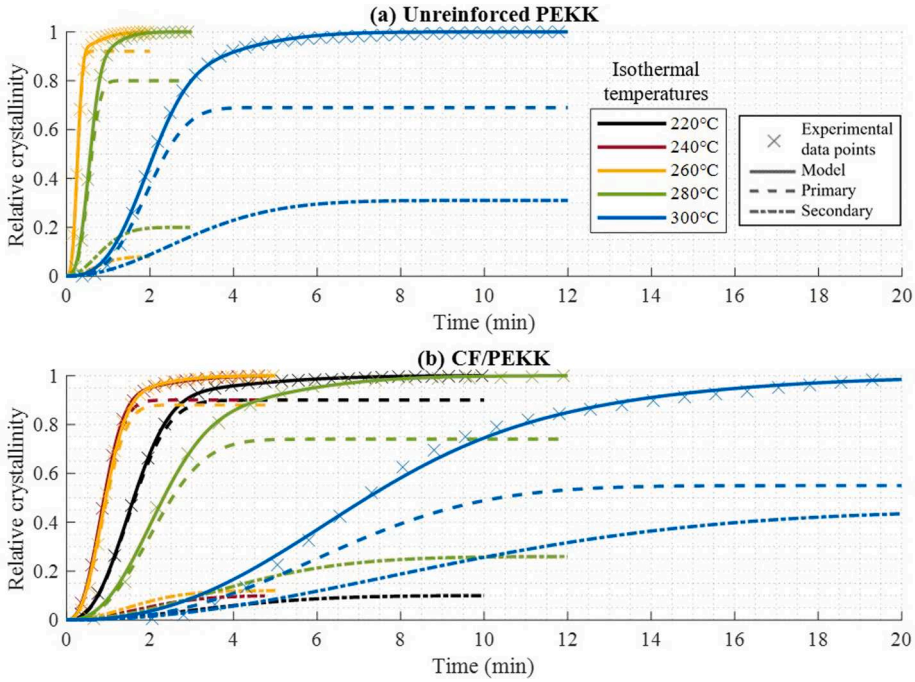

Fig. 13. Relative crystallinity against time of (a) unreinforced PEKK and (b) CF/PEKK at different isothermal holds, showing a comparison of the Velisaris-Seferis model with the experimental data, as well as the contribution of primary and secondary crystallisation mechanisms to the model.

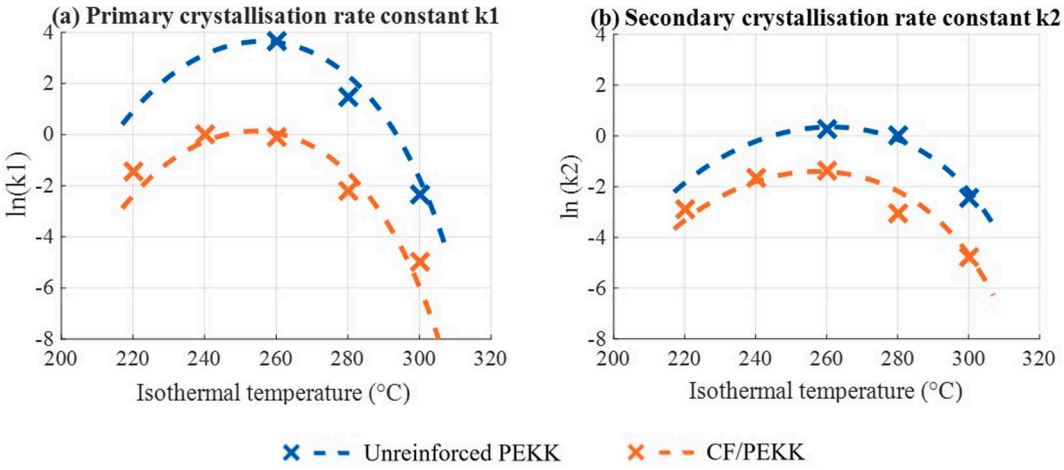

Fig. 14. Logarithmic plot of (a) k_1 and (b) k_2 against isothermal temperature for unreinforced PEKK and CF/PEKK. Dotted lines show the Hoffmann-Lauritzen models fitted to the experimental data.

Table 3
Parameters used for Hoffmann-Lauritzen modelling.

Parameters	Unreinforced PEKK	CF/PEKK
U^* (J mol^{-1})	4700 (Ref [17])	4700 (Ref [17])
R (m^3 Pa K^{-1} mol^{-1})	8.314	8.314
T_m^0 (used for T_∞, ΔT and f) (°C)	356 (Ref [16])	356 (Ref [16])
T_∞ (°C)	131	131
k_{01} (min^{-3})	1.500×10^{14}	1.5460×10^{13}
k_{02} (min^{-2})	5.041×10^{7}	3.593×10^{7}
K_{g1} (K^2)	2.486×10^{5}	2.687×10^{5}
K_{g2} (K^2)	2.025×10^{5}	2.359×10^{5}

with increasingly faster cooling rates. An LTE or a small shoulder at slow cooling rates has been observed in literature for PEEK [24,29,30], however PEEK possesses a more linear structure than any grade of PEKK, resulting in faster chain-packing and therefore a faster secondary crystallisation mechanism.

Fig. 16 shows SEM images of cryofractured CF/PEKK samples after undergoing 5 °C/min and 100 °C/min cooling rates respectively, with high and low crystallinities. Fig. 16a shows highly coated fibres, whereas clean, exposed fibres are observed in the lower crystallinity case in Fig. 16b. Similar behaviour has been observed in CF/PEEK in published literature [5,41]. This suggests that higher crystallinity in the matrix will improve fibre–matrix adhesion when compared to a more amorphous matrix.

3.2.2. Crystallisation kinetics at different cooling rates

Fig. 17 shows heat flow – temperature thermograms of PEKK and CF/PEKK samples while undergoing different cooling rates, showing melt crystallisation exotherms as the material cools and solidifies.

In both unreinforced PEKK and CF/PEKK composite, crystallisation takes place at progressively lower temperatures with faster cooling rates. At slower rates, chains have more time to move, and therefore begin to crystallise at higher temperatures. As the cooling rate is progressively increased, the polymer begins diffusion at lower temperatures.

Comparing PEKK and CF/PEKK, the composite samples in Fig. 17b consistently begin crystallisation at lower temperatures than their neat counterparts in Fig. 17a. The introduction of carbon fibres clearly obstructs the crystallisation mechanism of the matrix, resulting in a delayed crystallisation compared to unreinforced PEKK. This progressively lowers the total crystallinity developed with faster cooling rates, as discussed in the previous section. The crystallisation peak completely disappears at the fastest cooling rates for CF/PEKK in Fig. 17b, whereas unreinforced PEKK in Fig. 17a still shows a crystallisation peak at 150 °C/min cooling rate.

3.2.3. Modelling of non-isothermal crystallisation kinetics

Similar to isothermal crystallisation kinetics, relative crystallinity plots of each sample are required to implement any model. Using Eq. (3.1), such a plot is obtained, shown in Fig. 18. The kinetics for CF/PEKK at 150 °C/min are not evaluated, as the achieved crystallinity was very low (0.7%). Note that, while all samples reach a relative volume crystallinity of 1 in Fig. 18, this does not mean that all samples achieved the same level of absolute crystallinity (listed in Table 4). As observed in Section 3.2.2, unreinforced PEKK undergoes a faster crystallisation than its composite counterpart for each given cooling rate.

As discussed in Section 1, Avrami-based modelling includes the temperature-dependent crystallisation rate constant k. Therefore, creating an Avrami plot as shown in Fig. 12 (by plotting $\ln[-\ln(1-\alpha)]$ against $\ln(t)$) in order to find information on the possible primary crystallisation mechanism (a value for n_1) is not suitable in this instance, now that k varies with temperature under non-isothermal conditions.

Further to this, changing the thermal cycle that the sample undergoes is not likely to change the spherulitic (or otherwise) nature of crystallisation, but rather the extent to which it occurs (the total crystallinity achieved). Therefore, n_1 and n_2 have been kept the same as in Section 3.1.3: $n_1 = 3$ and $n_2 = 2$ for unreinforced PEKK; and $n_1 = 2.5$ and $n_2 = 2$ for CF/PEKK composite.

In order to model dynamic behaviour, the dual Nakamura model, Eq. (1.6), presented in Section 1 was scripted in MATLAB. Substituting k_1 and k_2 with Hoffmann-Lauritzen model Eqs. (3.3) and (3.5) yields the following model:

$$\alpha(t) = w_1\left(1 - exp\left[-\left(\int_0^t \left(k_{01}\left[\exp\left(-\frac{3U^*}{R(T-T_\infty)}\right)\times\exp\left(-\frac{3K_{g1}}{T\Delta Tf}\right)\right]\right)^{1/n_1} dt\right)^{n_1}\right]\right) + w_2\left(1 - exp\left[-\left(\int_0^t \left(k_{02}\left[\exp\left(-\frac{2U^*}{R(T-T_\infty)}\right)\times\exp\left(-\frac{2K_{g2}}{T\Delta Tf}\right)\right]\right)^{1/n_2} dt\right)^{n_2}\right]\right) \quad (3.6)$$

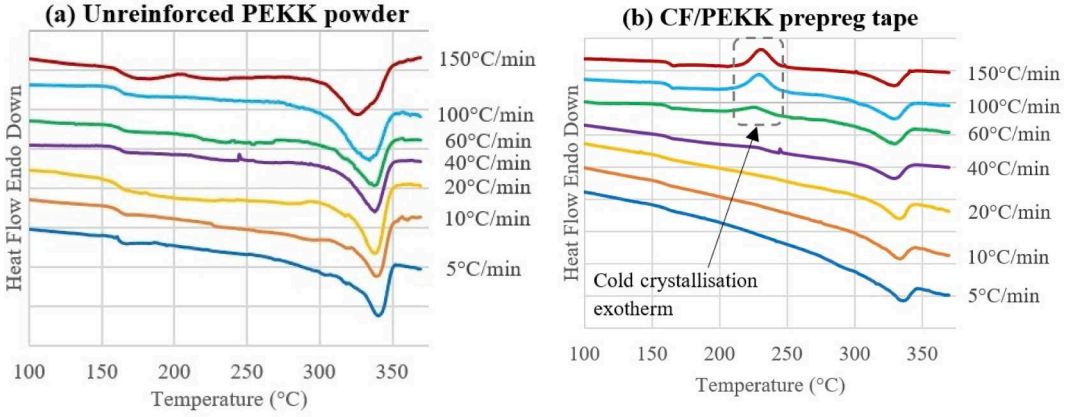

Fig. 15. DSC thermograms of (a) unreinforced PEKK and (b) CF/PEKK prepreg at 20 °C/min heat ramp after different cooling rates.

Table 4
Average values for transition temperatures, enthalpies and total crystallinity of PEKK powder and CF/PEKK prepreg tape after undergoing different cooling rates.

Cooling rate (°C/min)	Unreinforced PEKK					
	T_g (°C)	T_{cc} (°C)	ΔH_{cc} (J/g)	T_m (°C)	ΔH_m (J/g)	χ (%)
5	160.9 ± 0.8	–	–	341.5 ± 1.5	33.1 ± 0.3	25.5 ± 0.2
10	161.1 ± 0.7	–	–	340.0 ± 1.2	29.2 ± 3.1	22.5 ± 2.5
20	162.8 ± 1.8	–	–	338.0 ± 0.3	27.2 ± 0.1	20.9 ± 0.1
40	164.0 ± 1.9	–	–	337.4 ± 0.4	28.3 ± 1.0	21.8 ± 0.8
60	161.4 ± 0.1	–	–	337.0 ± 0.4	27.4 ± 1.2	21.1 ± 0.9
100	161.9 ± 0.7	212.3 ± 4.7	0.6 ± 0.2	331.9 ± 2.4	26.2 ± 0.6	19.7 ± 0.3
150	159.5 ± 3.9	210.9 ± 8.7	1.9 ± 0.1	326.0 ± 0.8	26.7 ± 0.4	19.0 ± 0.2
CF/PEKK						
5	159.2 ± 1.8	–	–	334.4 ± 0.7	10.6 ± 0.0	25.7 ± 0.0
10	160.6 ± 3.6	–	–	335.0 ± 2.2	7.8 ± 0.7	18.9 ± 1.6
20	158.8 ± 3.0	–	–	334.9 ± 2.5	7.0 ± 0.0	16.9 ± 0.2
40	161.9 ± 1.5	–	–	333.1 ± 4.6	6.6 ± 0.7	16.1 ± 0.6
60	161.2 ± 0.1	222.0 ± 4.2	2.1 ± 1.6	333.2 ± 3.3	7.8 ± 1.6	14.0 ± 0.1
100	162.8 ± 0.8	226.8 ± 2.2	5.8 ± 1.3	331.9 ± 3.5	8.7 ± 1.4	6.8 ± 0.1
150	162.0 ± 1.4	226.1 ± 4.7	7.7 ± 0.4	330.9 ± 1.8	8.3 ± 0.7	1.5 ± 0.8

T_g: Glass transition temperature.
T_{cc}: Cold crystallisation temperature.
ΔH_{cc}: Cold crystallisation enthalpy.
Tm: High temperature endotherm enthalpy.
ΔH_m: Melting enthalpy.
χ: Total crystallinity.

T is the temperature at time t, dependent on the cooling rate r:

$$T = T_m - rt \tag{3.7}$$

where T_m is the melt temperature from which the cooling begins (in this case, 370 °C).

3.2.3.1. Unreinforced PEKK. The heat scan curves of unreinforced PEKK in Fig. 15 show a single melting endotherm, and therefore values for w_1 and w_2 cannot be set according to LTE:HTE ratios as in the isothermal modelling. Therefore, the ratio of w_1 and w_2 was optimised by the script. The resulting fits are shown in Fig. 19. These show a decreasing contribution of secondary crystallisation as the cooling rate increases, in line with the observations by Bessard et al. [24] and Regis et al. [29] on the presence of secondary crystallisation under non-isothermal crystallisation. The resulting variation of w_1 and w_2 with cooling rate is shown in Fig. 20.

The model can be adapted to account for this variation in w_1 by introducing Eq. (3.8) (obtained from the fit in Fig. 20) in Eq. (3.6) and remembering that $w_1 + w_2 = 1$.

$$w_1 = -1.399r^{-0.8707} + 1 \tag{3.8}$$

where r is the applied cooling rate.

The contribution of w_2 necessary to achieve a better fit in the models above suggests that there may be some secondary crystallisation taking place in the material, despite no presence of an LTE endotherm in Fig. 15a. While the LTE:HTE ratio may be a good estimate of primary and secondary crystallisation content in the case of isothermal studies, this is not the case in non-isothermal studies. Therefore, a LTE may not be the sole indicator of presence of secondary crystallisation in PEKK.

3.2.3.2. CF/PEKK composite. In the case of CF/PEKK composite, performing the fitting while allowing the script to optimise the values of w_1 and w_2 resulted in $w_1 = 1$ for all curves. It is likely that only primary crystallisation occurs in the case of CF/PEKK, now that kinetics are slower than in unreinforced PEKK and there may not be enough time for the slower secondary crystallisation mechanism to take place.

Even when only accounting for primary crystallisation, however, the model underpredicts the kinetics of the composite, and at increasingly faster rates the crystallinity achieved in the experiments is not reached by the model. This is shown in Fig. 21. This may be due to the crystallisation rate equation for k_1 (Eq. (3.4)) underestimating the crystallisation capability of the polymer under non-isothermal conditions, particularly at higher cooling rates. Including a secondary crystallisation step would only delay kinetics further, as this is a slower mechanism than primary crystallisation.

In order to successfully model dynamic crystallisation of composite PEKK, a z coefficient was introduced to Eq. (3.6), which was optimised by the MATLAB script. This coefficient is bespoke for the specific grade of composite PEKK, as it would be beneficial to use for instance in the modelling of crystallinity development across a laminate experiencing different temperature gradients and distributions.

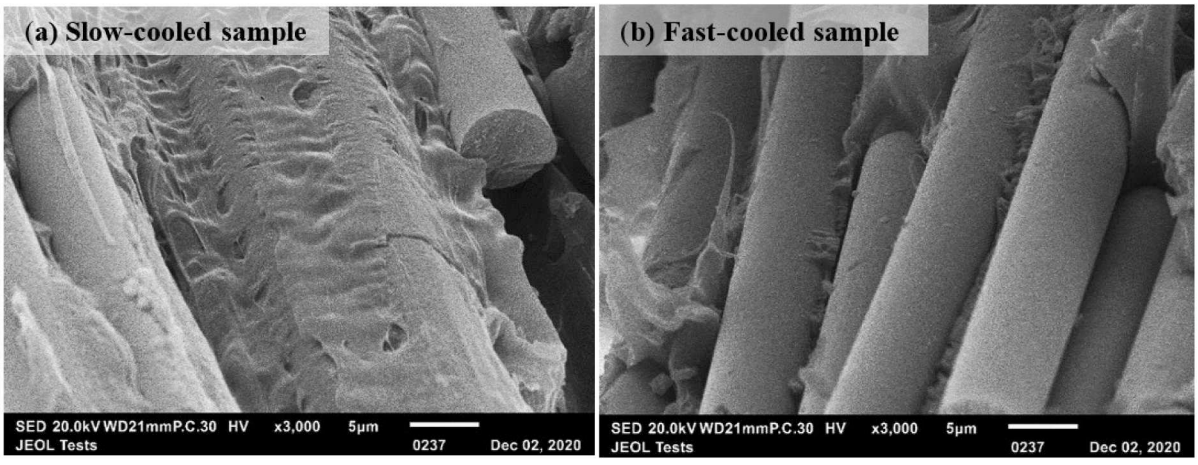

Fig. 16. SEM of cryofractured CF/PEKK sample after undergoing a cooling rate of (a) 5 °C/min from the melt to room temperature (25.6% crystallintiy) and (b) 100 °C/min from the melt to room temperature (6.9% crystallinity).

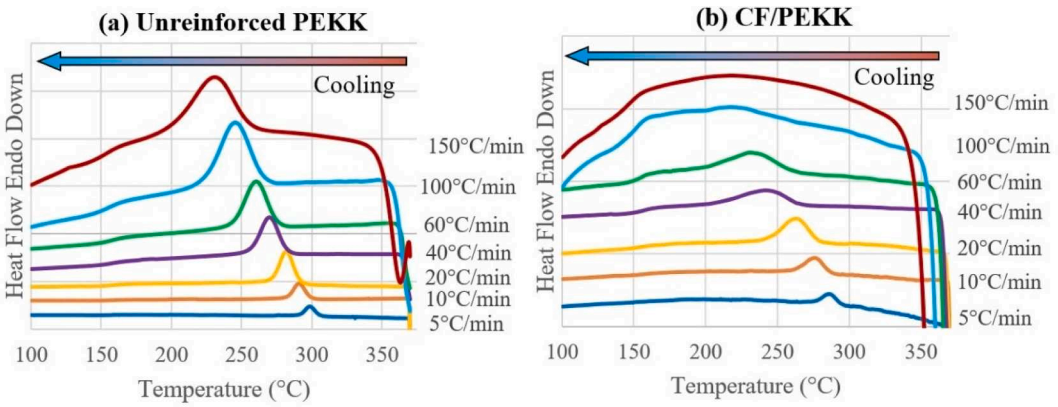

Fig. 17. DSC thermograms of (a) Unreinforced PEKK powder and (b) CF/PEKK prepreg tape while undergoing different cooling rates.

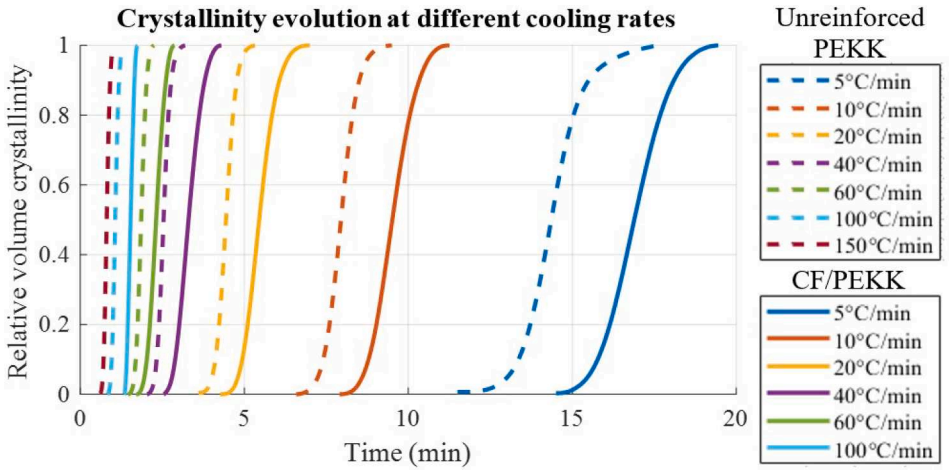

Fig. 18. Relative crystallinity against time of unreinforced PEKK (dotted lines) and CF/PEKK (solid lines) at different cooling rates.

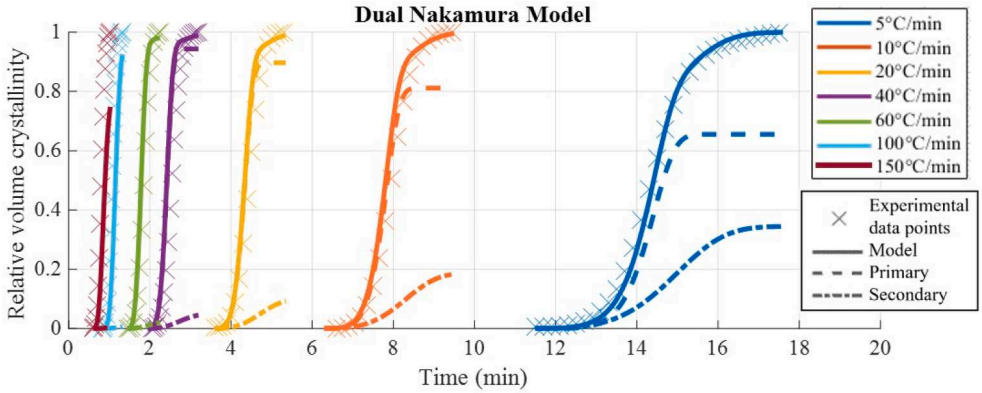

Fig. 19. Dual Nakamura model fits to non-isothermal crystallisation experimental data of unreinforced PEKK powder undergoing a range of cooling rates.

Since, as discussed above, $w_1 = 1$ and $w_2 = 0$, the second half of Eq. (3.6) can be ignored, and becomes:

$$\alpha(t) = z\left(1 - \exp\left[-\left(\int_0^t \left(k_{01}\left[\exp\left(-\frac{3U^*}{R(T-T_\infty)}\right)\times\exp\left(-\frac{3K_{g1}}{T\Delta Tf}\right)\right]\right)^{1/n_1} dt\right)^{n_1}\right]\right) \tag{3.9}$$

The expression obtained for z is shown in Eq. (3.10), where r is the cooling rate, and the resulting fittings are shown in Fig. 22.

$$z = 0.00229\exp(0.109r) + 1 \tag{3.10}$$

3.3. End-use applicability

It is of interest to reflect on which of the studied processing conditions would result in the best performance of CF/PEKK composites within the context of high-performance applications. To determine this, a structure–property correlation has to be established via manufacturing and mechanical testing. As this is outside the scope of the current work,

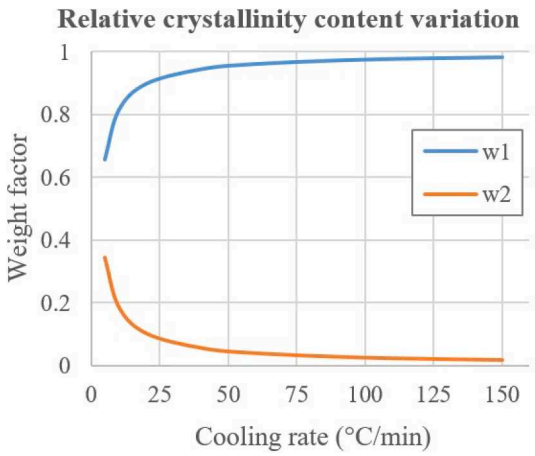

Fig. 20. Variation of crystallisation relative content (w_1 and w_2) with cooling rate for crystallisation kinetics modelling of unreinforced PEKK powder.

the remainder of this discussion will be based on the understanding of crystallinity that has been developed in this article, as well as the existing understanding of crystalline morphology from literature.

A high crystallinity content may be desirable [1,4] in order to achieve specific performance requirements, such as high strength, stiffness, or chemical resistance, which usually entails using slow cooling rates or isothermal holds. Deciding what isothermal temperature hold or cooling rate will result in a better response is therefore worth investigating and discussing. In this work, different applied thermal cycles have been observed to influence the formation of crystals. Some literature has reported that larger spherulite sizes reduce the mechanical performance of PEEK [30,42] and other polymers [43,44]. Larger crystal sizes in PEKK and CF/PEKK are shown here to develop at high isothermal hold temperatures, and are also likely developed at slow cooling rates (crystallisation takes place at higher temperatures with slower rates, as seen in Fig. 17). This suggests lower isothermal holds, in the range of 220–260 °C, may result in improved mechanical properties, and may therefore be more attractive to designers and manufacturers. The higher end of this range (240–260 °C), while resulting in larger spherulites, will undergo faster crystallisation kinetics, which may lead to shorter processing times. Time-temperature-transformation diagrams based on the isothermal Velisaris-Seferis modelling have been included in Fig. 23, which allow for the relative crystallinity of the material to be determined at any holding temperature and time. A relative crystallinity of 1 means the material has reached its full crystallisation potential, absolute percentage values of which are presented in Table 1.

Time-temperature transformation diagrams have also been included for non-isothermal instances in Fig. 24, based on the performed Nakamura modelling. In this instance, a relative crystallinity of 1 refers to the crystallinity achieved by cooling at 5 °C/min (absolute crystallinity of 25.5% and 25.7% for unreinforced and composite PEKK respectively). As faster cooling rates are performed (indicated by the labelled slopes), lower crystallinities are achieved, as outlined in Table 4.

It is worth considering, however, that holding temperature or cooling rate are not the only factors influencing physical and mechanical properties. The melt temperature will have a large effect on resin flow and part consolidation, as will the application of sufficient processing pressure, without which defects like voids or non-homogeneous consolidation may arise, possibly impacting mechanical performance. Further to this, the experiments performed in this work have all focussed on small amounts of material under the highly controlled, inert environment that DSC provides. This may not be directly applicable to an industrial manufacturing setting, where larger parts are unlikely to undergo highly controlled cooling and may experience a temperature

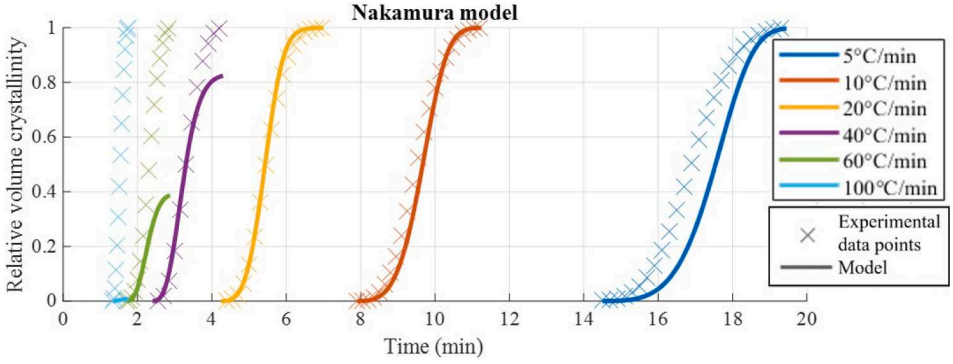

Fig. 21. Single Nakamura model fits to non-isothermal crystallisation experimental data of CF/PEKK composite undergoing a range of cooling rates.

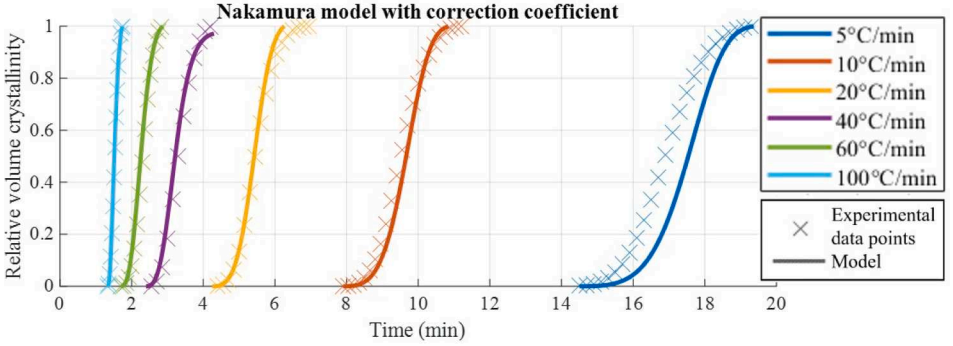

Fig. 22. Single Nakamura with correction coefficient fits to non-isothermal crystallisation experimental data of CF/PEKK composite undergoing a range of cooling rates.

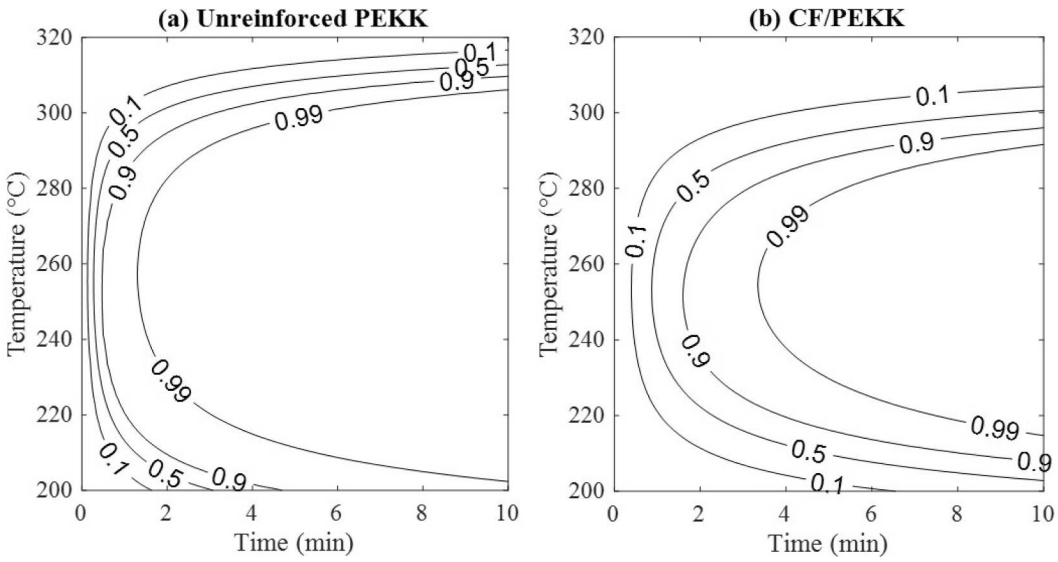

Fig. 23. Time-temperature-transformation diagrams of relative crystallinity development for (a) unreinforced PEKK and (b) CF/PEKK at different isothermal holds. A relative crystallinity of 1 means the material has achieved its full crystallisation potential, based on the crystallinity values shown in Table 1.

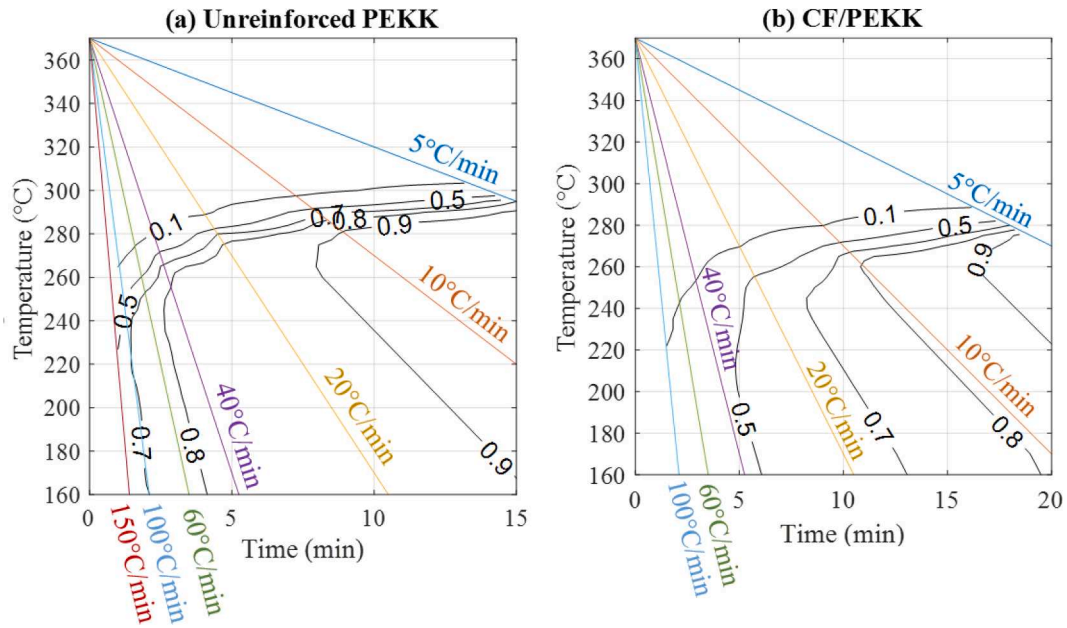

Fig. 24. Time-temperature-transformation diagrams of relative crystallinity development for (a) unreinforced PEKK and (b) CF/PEKK when undergoing different cooling rates. The coloured straight lines denote the performed cooling rates in this study. A relative crystallinity of 1 refers to the total crystallinity achieved after cooling at 5 °C/min.

gradient across their thickness. The results in this work will, however, form a solid guideline for industrial-scale processing of CF/PEKK composite parts.

4. Conclusions

When undergoing non-isothermal crystallisation, PEKK in unreinforced form crystallises even at the fastest cooling rate tested in this study (150 °C/min, achieving partial crystallisation), whereas CF/PEKK, possessing slower crystallisation kinetics, remains amorphous at the fastest cooling rate. Fibre-matrix adhesion is enhanced in more crystalline samples than in amorphous ones, as observed in cryofractured CF/PEKK samples. During dynamic crystallisation, the secondary crystallisation behaviour is not obvious, due to the slower nature of this mechanism. Slow-cooled CF/PEKK samples with higher levels of crystallinity were observed to have a stronger fibre–matrix interphase than amorphous (fast-cooled) samples, as examined by SEM.

Crystallisation kinetics for both isothermal and non-isothermal conditions have been studied using Avrami-based models, where two parallel Avrami-based expressions are used to account for primary and secondary crystallisation respectively. For the isothermal instances, the Velisaris-Seferis model was implemented, and a correlation between the isothermal holding temperature and the crystallisation rate constants was established. This was then used in the non-isothermal crystallisation cases in the implementation of adapted versions of the Nakamura model: a dual Nakamura model with a decreasing contribution of secondary crystallisation with faster cooling rates for unreinforced PEKK, and a single Nakamura model with a material-specific correction factor for

CF/PEKK. Successful fits were achieved in all instances, which will allow for the prediction of crystallisation evolution at other different rates and isothermal holds.

Overall, the findings of this work lead to a better understanding of the effect that different processing cycles might have on crystal structure development in CF/PEKK composite parts. Given the results in this work, a preliminary isothermal holding temperature range that provides optimum spherulitic development for its intended application in high-performance environments is found at 220–260 °C. The limitations of this work within the context of industrial applications must, however, be taken into account, namely the differences in scale, processing parameters and environment control when comparing small scale DSC studies and industrial-scale manufacturing.

CRediT authorship contribution statement

Helena Pérez-Martín: Conceptualization, Investigation, Formal analysis, Project administration, Writing – original draft. **Paul Mackenzie:** Supervision, Resources, Writing – review & editing. **Alex Baidak:** Supervision, Resources, Writing – review & editing. **Conchúr M. Ó Brádaigh:** Supervision, Resources, Writing – review & editing. **Dipa Ray:** Conceptualization, Supervision, Resources, Project administration, Writing – review & editing.

Declaration of Competing Interest

The authors declare that they have no known competing financial interests or personal relationships that could have appeared to influence the work reported in this paper.

Acknowledgements

The authors acknowledge the financial support received from the National Manufacturing Institute for Scotland (NMIS-IDP/009) and Hexcel Composites Limited.

References

[1] Comer AJ, Ray D, Obande WO, Jones D, Lyons J, Rosca I, et al. Mechanical characterisation of carbon fibre–PEEK manufactured by laser-assisted automated-tape-placement and autoclave. Compos Part Appl Sci Manuf 2015;69:10–20.
[2] Pérez-Martín H, Mackenzie P, Baidak A, Ó Brádaigh CM, Ray D. Crystallinity studies of PEKK and carbon fibre/PEKK composites: a review. Compos Part B Eng 2021;223:109127. https://doi.org/10.1016/j.compositesb:2021.109127.
[3] Flanagan M, Goggins J, Doyle A, Weafer B, Ward M, Bizeul M, et al. Out-of-autoclave manufacturing of a stiffened thermoplastic carbon fibre PEEK panel. In: AIP Conf Proc 2017;1896. 10.1063/1.5008001.
[4] Choupin T, Debertrand L, Fayolle B, Régnier G, Paris C, Cinquin J, et al. Influence of thermal history on the mechanical properties of poly(ether ketone ketone) copolymers. Polym Cryst 2019;2(6). https://doi.org/10.1002/pcr2.v2.610.1002/pcr2.10086.
[5] Gao S-L, Kim J-K. Cooling rate influences in carbon fibre/PEEK composites. Part I. Crystallinity and interface adhesion. Compos Part Appl Sci Manuf 2000;31:517–30. https://doi.org/10.1016/S1359-835X(00)00009-9.
[6] Gao S-L, Kim J-K. Cooling rate influences in carbon fibre/PEEK composites. Part II: interlaminar fracture toughness. Compos A Appl Sci Manuf 2001;32(6):763–74.
[7] Deignan A, Stanley WF, McCarthy MA. Insights into wide variations in carbon fibre/polyetheretherketone rheology data under automated tape placement processing conditions. J Compos Mater 2018;52(16):2213–28. https://doi.org/10.1177/0021998317740733.
[8] Lee Y, Porter RS. Crystallization of poly(etheretherketone) (PEEK) in carbon fiber composites. Polym Eng Sci 1986;26(9):633–9. https://doi.org/10.1002/pen.760260909.
[9] Gardner KH, Hsiao BS, Faron KL. Polymorphism in poly (aryl ether ketone). Polymer 1994;35:2290–5. https://doi.org/10.1016/0032-3861(94)90763-3.
[10] Tencé-Girault S, Quibel J, Cherri A, Roland S, Fayolle B, Bizet S, et al. Quantitative Structural Study of Cold-Crystallized PEKK. ACS Appl Polym Mater 2021;3(4):1795–808. https://doi.org/10.1021/acsapm.0c0138010.1021/acsapm.0c01380.s001.
[11] Choupin T, Fayolle B, Régnier G, Paris C, Cinquin J, Brulé B. Isothermal crystallization kinetic modeling of poly(etherketoneketone) (PEKK) copolymer. Polymer 2017;111:73–82. https://doi.org/10.1016/j.polymer.2017.01.033.
[12] Quiroga Cortés L, Caussé N, Dantras E, Lonjon A, Lacabanne C. Morphology and dynamical mechanical properties of poly ether ketone ketone (PEKK) with meta phenyl links. J Appl Polym Sci 2016;133(19):n/a–. https://doi.org/10.1002/app.43396.
[13] Hsiao BS, Chang IY, Sauer BB. Isothermal crystallization kinetics of poly(ether ketone ketone) and its carbon-fibre-reinforced composites. Polymer 1991;32(15):2799–805. https://doi.org/10.1016/0032-3861(91)90111-U.
[14] Gardner KH, Hsiao BS, Matheson RR, Wood BA. Structure, crystallization and morphology of poly (aryl ether ketone ketone). Polymer 1992;33(12):2483–95. https://doi.org/10.1016/0032-3861(92)91128-O.
[15] Arkema. Introduction to ultra high-performance Kepstan® PEKK 2020.
[16] Chang IY, Hsiao BS. Thermal properties of high performance thermoplastic composites based on poly(ether ketone ketone). In: (PEKK). 36th Int SAMPE Symp; 1991. p. 1587–601.
[17] Choupin T, Fayolle B, Régnier G, Paris C, Cinquin J, Brulé B. A more reliable DSC-based methodology to study crystallization kinetics: Application to poly(ether ketone ketone) (PEKK) copolymers. Polymer 2018;155:109–15. https://doi.org/10.1016/j.polymer.2018.08.060.
[18] Ho R-M, Cheng SZD, Hsiao BS, Gardner KH. Crystal morphology and phase identifications in poly(aryl ether ketone)s and their copolymers. 1. Polymorphism in PEKK. Macromolecules 1994;27(8):2136–40. https://doi.org/10.1021/ma00086a023.
[19] Ho RM, Cheng SZD, Hsiao BS, Gardner KH. Crystal morphology and phase identifications in poly(aryl ether ketone)s and their copolymers. 3. Polymorphism in a polymer containing alternated terephthalic acid and isophthalic acid isomers. Macromolecules 1995;28:1938–45. https://doi.org/10.1021/ma00110a030.
[20] Jin L, Ball J, Bremner T, Sue H-J. Crystallization behavior and morphological characterization of poly(ether ether ketone). Polymer 2014;55(20):5255–65. https://doi.org/10.1016/j.polymer.2014.08.045.
[21] Painter PC, Coleman MM. Polymer Morphology. Fundam. Polym. Sci. Introd. Text. 2nd ed. Routledge; 1997, p. 250–3.
[22] Hsiao BS, Gardner KH, Cheng SZD. Crystallization of poly(aryl ether ketone ketone) copolymers containing terephthalate/isophthalate moieties. J Polym Sci Part B Polym Phys 1994;32:2585–94. https://doi.org/10.1002/polb.1994.090321604.
[23] Bassett D, Olley R, Alraheil I. On crystallization phenomena in PEEK. Polymer 1988;29(10):1745–54. https://doi.org/10.1016/0032-3861(88)90386-2.
[24] Bessard E, De Almeida O, Bernhart G. Unified isothermal and non-isothermal modelling of neat PEEK crystallization. J Therm Anal Calorim 2014;115(2):1669–78. https://doi.org/10.1007/s10973-013-3308-8.
[25] Blundell DJ, Osborn BN. The morphology of poly(aryl-ether-ether-ketone). Polymer 1983;24(8):953–8. https://doi.org/10.1016/0032-3861(83)90144-1.
[26] Cebe P, Hong S-D. Crystallization behaviour of poly(ether-ether-ketone). Polymer 1986;27(8):1183–92. https://doi.org/10.1016/0032-3861(86)90006-6.
[27] Lattimer MP, Hobbs JK, Hill MJ, Barham PJ. On the origin of the multiple endotherms in PEEK. Polymer 1992;33(18):3971–3. https://doi.org/10.1016/0032-3861(92)90391-9.
[28] Tardif X, Pignon B, Boyard N, Schmelzer JWP, Sobotka V, Delaunay D, et al. Experimental study of crystallization of PolyEtherEtherKetone (PEEK) over a large temperature range using a nano-calorimeter. Polym Test 2014;36:10–9. https://doi.org/10.1016/j.polymertesting.2014.03.013.
[29] Regis M, Zanetti M, Pressacco M, Bracco P. Opposite role of different carbon fiber reinforcements on the non-isothermal crystallization behavior of poly (etheretherketone). Mater Chem Phys 2016;179:223–31. https://doi.org/10.1016/j.matchemphys.2016.05.034.
[30] Lustiger A, Uralil FS, Newaz GM. Processing and structural optimization of PEEK composites. Polym Compos 1990;11(1):65–75. https://doi.org/10.1002/pc.750110109.
[31] Avrami M. Kinetics of phase change. I: General theory. J Chem Phys 1939;7(12):1103–12. https://doi.org/10.1063/1.1750380.
[32] Velisaris CN, Seferis JC. Crystallization kinetics of polyetheretherketone (peek) matrices. Polym Eng Sci 1986;26(22):1574–81. https://doi.org/10.1002/pen.760262208.
[33] Cowie JMG. The crystalline state: Kinetics of crystallization. In: Polym. Chem. Phys. Mod. Mater. 2nd ed. Blackie Academic & Professional; 1998.
[34] Hoffman JD, Lauritzen JI. Crystallization of bulk polymers with chain folding: theory of growth of lamellar spherulites. J Res Natl Bur Stand Sect Phys Chem 1961;65A(4):297. https://doi.org/10.6028/jres.065A.035.
[35] Chelaghma SA, De Almeida O, Margueres P, Passieux J-C, Perie J-N, Vinet A, et al. Identification of isothermal crystallization kinetics of poly(ether-ketone-ketone)

based on spherulite growth measurements and enthalpic data. Polymer Crystallization 2020;3(4). https://doi.org/10.1002/pcr2.v3.410.1002/pcr2.10141.
[36] Cebe P. Application of the parallel Avrami model to crystallization of poly (etheretherketone). Polym Eng Sci 1988;28(18):1192–7. https://doi.org/10.1002/pen.760281809.
[37] Nakamura K, Katayama K, Amano T. Some aspects of nonisothermal crystallization of polymers. II. Consideration of the isokinetic condition. J Appl Polym Sci 1973;17:1031–41. https://doi.org/10.1002/app.1973.070170404.
[38] Harris L. A study of the crystallisation kinetics on PEEK and PEEK composites. University of Birmingham, 2011.
[39] Choupin T. Mechanical performances of PEKK thermoplastic composites linked to their processing parameters. École nationale supérieure d'arts et métiers, 2017.
[40] Arkema. Kepstan® PEKK Brochure 2018.
[41] Saiello S, Kenny J, Nicolais L. Interface morphology of carbon fibre/PEEK composites. J Mater Sci 1990;25(8):3493–6. https://doi.org/10.1007/BF00575375.
[42] Chu J-N, Schultz JM. The influence of microstructure on the failure behaviour of PEEK. J Mater Sci 1990;25(8):3746–52. https://doi.org/10.1007/BF00575414.
[43] Ehrenstein GW, Theriault RP. Polymeric Materials: Structure, Properties, Applications. Hanser Publishers; 2001.
[44] Starkweather Jr HW, Brooks RE. Effect of spherulites on the mechanical properties of nylon 66. J Appl Polym Sci 1959;1:236–9. https://doi.org/10.1002/app.1959.070010214.